CHAPTER FIVE

OPTICAL CHARACTERISTICS

5.1 Introduction

The optical behaviour of a semiconductor material can be determined from the spectral dependence of the real and imaginary parts of the refractive index. These parts are most readily determined by measuring the transmission and/or the reflection of a plane-parallel slab as a function of the incident photon energy. The dependence of refractive index on photon energy, as the fundamental absorption is approached from the long wavelength limit, contains information on inter-band electronic transitions occurring at higher energies and hence should be relatable to the density of electronic states. The dielectric function, which is strongly dependent on the refractive index, has been used [104-107] to help in understanding covalent and ionic bonding in a wide class of materials and empirical relationships have been deduced between refractive indices and the structural and chemical quantities which characterize a material, viz., coordination number and chemical valency. Another important parameter to characterize the material optically is the absorption coefficient, which is, actually, related to the imaginary part of the refractive index. The variation of the absorption coefficient with the incident photon energy is sufficient to give information on the possible optical transitions of an electron from the valence to the conduction bands across the energy band gap. The rapid increase in the absorption coefficient at a

particular small range of incident photon energy can be used to estimate the energy gap of the material.

The optical properties have been studied experimentally as well as theoretically for ZnS [5-11] and ZnSe [20, 21, 27-29] materials. Meanwhile, the optical behaviour of ZnS_xSe_{1-x} system has not been intensively and comprehensively studied. However, a few studies have been reported [41- 43, 46, 49, 51-53, 108, 109] on the optical behaviour of these materials prepared by different techniques.

In this chapter, the optical transmission measurements used to investigate the optical characteristics of ZnS_xSe_{1-x} thin films prepared by electron beam evaporation onto glass substrates at 60 ° C will be described. The two parts of both refractive index and dielectric function were studied as a function of the incident photon energy, composition and thickness of the film. The empirical relations in the dielectric theory were used to estimate the characteristic energies such as Penn energy gap, plasma energy, Fermi energy, the average energy of the valence electrons, the energy of the effective dispersion oscillator and the dispersion energy. The fundamental optical energy gap was estimated by fitting the absorption coefficient data in the high absorption region to the direct transition expression. The variation of the energy gap with the composition in the film was investigated. The shift in the energy gap caused by the uniaxial stress inside the film and the grain size effect was estimated for the samples studied in this work. Finally, the optical phonon energies associated with the indirect optical transitions were determined from the tail that was observed in the absorption coefficient data.

5.2 Optical transmission

Figure 5.1 (a-d) shows typical optical transmission spectra measured at normal incidence in the photon wavelength range of 200-2400 nm for ZnS_xSe_{1-x} thin films (samples S1, S7, S10 and S22) with sulfur composition x = 0.12, 0.78, 0.90 and 0.99 and thickness t = 2586, 828, 820 and 232 nm, respectively. The films were deposited by electron beam evaporation onto glass substrates at a temperature of almost 60 ° C and under pressure $\cong 10^{-5}$ torr. All the films studied in this work show high transparency, which is more than 75% in average, in the wavelength region of 700-3200 nm that is similar to the transparency range of ZnSe films prepared by electron beam and ion beam deposition reported in reference [21]. In this long wavelength limit the samples exhibited interference fringes. However, the number of the fringes in a certain range of λ depends on the thickness and the refractive index of the film. The structural features that appear in the transmission data near 2280, 2190, 1880 and 1380 nm in Figure 5.1 (a-d) are artifacts of the measurement arising from peculiarities of the spectrophotometer used for the measurement [83]; they are not related to the samples. Figure 5.2 demonstrates the transmission spectra in the wavelength range of the fundamental absorption edges for representative samples with different composition values. The onset of the optical absorption edge moves systematically towards shorter λ as x value increase i.e. the amount of sulfur increases in the sample.

5.3 Refractive index and dielectric function

The transmittance data were used to calculate the refractive index as described in chapter 3.The dispersion behaviour of the two parts of the complex refractive index n and k are shown in Figures 5.3 (a) and (b), respectively, for various samples with different compositional values. Similar curves were obtained for all of the samples

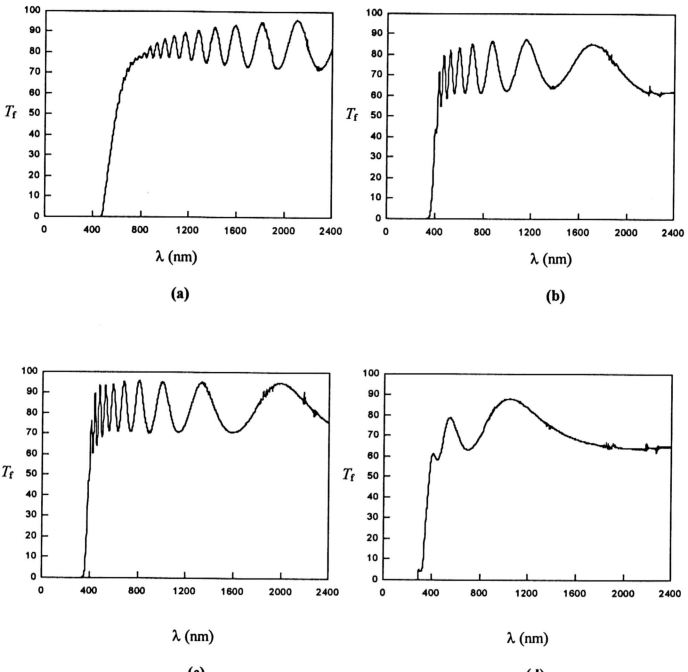

Figure 5.1: Transmission spectra, T_f %, versus the incident photon wavelength, λ, for ZnS_xSe_{1-x} thin films (samples S1, S7, S10 and S22) prepared by electron beam evaporation onto glass substrates at 60 °C with x values: 0.12 **(a)**, 0.78 **(b)**, 0.90 **(c)** and 0.99 **(d)**.

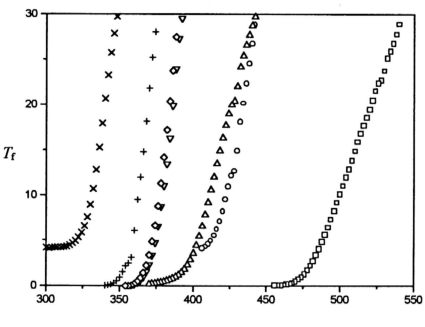

Figure 5.2: Transmission spectra, T_t%, versus the incident photon wavelength, λ, for ZnS_xSe_{1-x} thin films prepared by electron beam evaporation onto glass substrates at 60 ^{0} C with x values: 0.12 □ , 0.35 ○ , 0.41 △, 0.82 ▽, 0.90 ◇, 0.96 + and 0.99 ×.

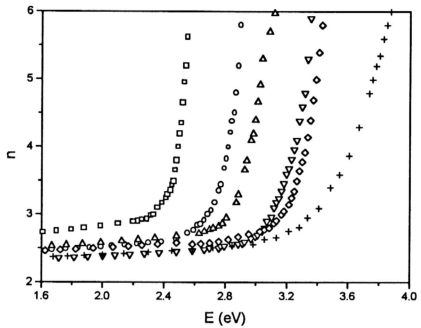

(a)

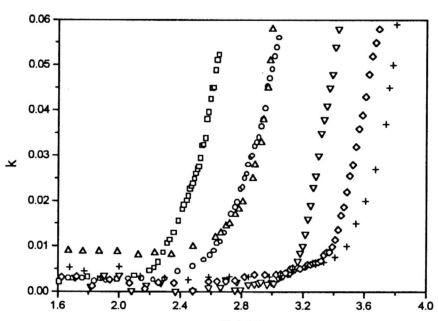

(b)

Figure 5.3: Dispersion of refractive index n **(a)** and extinction coefficient k **(b)** for ZnS_xSe_{1-x} thin films prepared by electron beam evaporation onto glass substrates at 60 ° C with x values: 0.12 □ , 0.35 ○, 0.41△ , 0.82 ▽, 0.90 ◇ and 0.99 +.

studied in this work, with the static refractive index $n(0)$ being approached at low energy limit of the incident photon and with n and k increasing drastically with increasing E as the fundamental optical absorption edge for each different sample is approached. Figure 5.4 (a) illustrates a plot of $n(0)$, as estimated from the extrapolation of $n(E)$ to long wavelength limit, versus x for ZnS_xSe_{1-x} films; these films have different values of thickness. Figure 5.4 (b), however, shows the dependence of $n(0)$ on film thickness for $ZnS_{0.9}Se_{0.1}$ samples.

The real and imaginary parts of the refractive index are strongly related to the complex dielectric function, $\varepsilon^*(E) = \varepsilon_1(E) + i\varepsilon_2(E)$, by the relation [110]

$$n^*(E) = n(E) - ik(E) = [\varepsilon^*(E)]^{1/2} \quad \text{.....(5.1)}$$

The optical constants $n(E)$ and $k(E)$, which have been determined from the transmission measurements, were used to determine $\varepsilon_1(E)$ and $\varepsilon_2(E)$ through the relations deduced from equation 5.1 such as

$$\varepsilon_1(E) = n^2(E) - k^2(E) \text{.....(5.2)}$$

$$\varepsilon_2(E) = 2n(E)k(E) \text{.....(5.3)}$$

Figures 5.5 (a) and (b) show the variation of ε_1 and ε_2, respectively, with E for different ZnS_xSe_{1-x} samples.

Refractive index dispersion data or the real part of the dielectric function below the inter-band absorption edge has been fitted to theoretical approximated expressions,

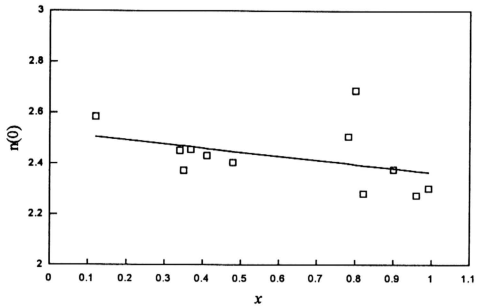

(a)

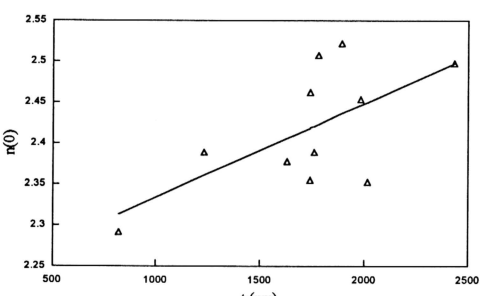

(b)

Figure 5.4: Static refractive index $n(0)$ versus x **(a)** for ZnS_xSe_{1-x} thin films and versus t **(b)** for $ZnS_{0.9}Se_{0.1}$ thin films prepared by electron beam evaporation onto glass substrates at 60 ° C.

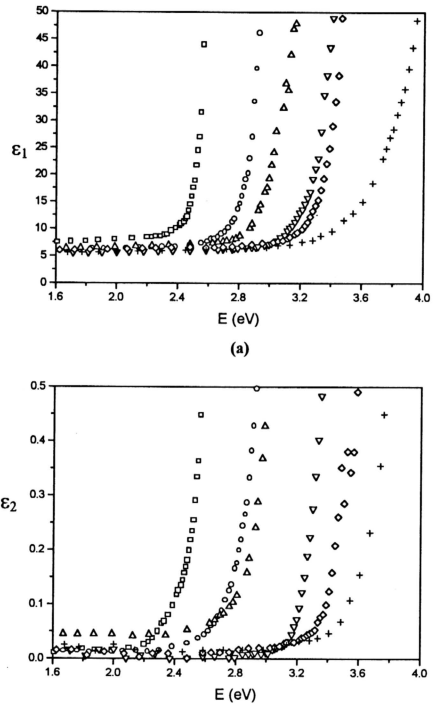

Figure 5.5: Real part ε_1 (a) and imaginary part ε_2 (b) of the dielectric function versus E for ZnS_xSe_{1-x} thin films prepared by electron beam evaporation onto glass substrates at 60 ° C with x values: 0.12 □, 0.35 ○, 0.41 △, 0.82 ▽, 0.90 ◇ and 0.99 +.

dealing with energy band calculations, by introducing certain physically meaningful parameters. These parameters are useful because they can assist in describing both crystal structure and ionicity of solids through their influence in the refractive index behaviour. Phillips and Vechten [104] have introduced an average energy gap "Penn gap", $\bar{E}_g$ which can be deduced from the static refractive index $n(0)$. Excitations of electrons across the average gap (actually across the fundamental gap) leads to absorption of the optical energy, and this is reflected in the refractive index through an effective valence plasma frequency as given by [87, 105]

$$[n(0)]^2 = 1+[\hbar\omega_p/\ \bar{E}_g]^2 \quad \text{.....(5.4)}$$

where $\hbar\omega_p$ is the plasma energy of the valence electrons (where $\hbar = h/2\pi$, and h is Planck's constant) with square of the plasma frequency $\omega_p^2 = 4\pi N_v e^2/m$, where N_v is the effective density of valence electrons (i. e number of valence electrons per unit volume), e and m are the charge and rest mass of the electron, respectively. Since ZnS_xSe_{1-x} films under investigation were found to exhibit zinc-blend structure with 8 atoms per unit cell, and in average each atom has 4 valence electrons, the valence electron density for such structure could be estimated as $N_v=32/a^3_0$, where a_0 is the lattice constant. Using the values of N_v, ω_p and hence $E_p = \hbar\omega_p$ were determined for the films and tabulated in Table 5.1. $\bar{E}_g$ was calculated for the films according to equation 5.4 and plotted in Figure 5.6 as a function of x. The $\bar{E}_g$ is not the principal optical gap E_g (to be discussed later) between the conduction and valence bands, but is an average gap between bonding and antibonding states. It is larger than E_g because it represents an average over the bands. The $\bar{E}_g$ is important for electrical properties of the material

Table 5.1: dispersion parameters for ZnS_xSe_{1-x} thin films prepared by electron beam evaporation onto glass substrates at 60 ° C.

Sample	x	E_p (eV)	E_p (eV)	E_B (eV)	E_w (eV)	E_0 (eV)	E_d (eV)	E_s (eV)
S1	0.12	15.50	16.27	15.51	25.54	4.55	25.82	9.30
S2	0.34	15.83	17.70	16.84	27.77	5.05	25.26	9.9
S3	0.35	15.90	18.46	17.60	28.98	5.45	25.26	10.01
S4	0.37	15.79	17.60	16.78	27.62	5.15	25.91	9.62
S5	0.41	15.94	18.00	17.17	28.26	5.44	26.66	9.54
S6	0.48	16.16	18.47	17.61	28.99	6.01	28.74	9.08
S7	0.78	16.45	17.89	17.05	28.07	5.08	26.86	10.07
S8	0.8	16.42	16.46	15.69	25.84	6.26	38.98	6.92
S9	0.82	16.48	20.07	19.13	31.50	6.27	26.42	10.27
S10	0.90	16.60	20.13	19.19	31.59	6.34	26.93	10.23
S11	0.90	16.59	19.11	18.22	30.00	6.04	28.44	9.68
S12	0.90	16.58	19.22	18.32	30.16	5.58	25.93	10.60
S13	0.90	16.54	19.40	18.50	30.45	5.66	25.70	10.64
S14	0.90	16.58	18.43	17.57	28.92	6.01	30.41	9.04
S15	0.90	16.58	19.11	18.22	29.99	6.04	28.44	9.67
S16	0.90	16.49	17.94	17.10	28.15	5.67	29.97	9.08
S17	0.90	16.60	17.92	17.09	28.13	5.92	31.74	8.68
S18	0.90	16.63	18.56	17.70	29.13	5.23	26.25	10.54
S19	0.90	16.62	19.52	18.61	30.64	6.01	27.23	10.15
S20	0.90	16.56	18.09	17.25	28.39	5.11	26.73	10.26
S21	0.96	16.65	20.39	19.44	32.00	6.20	25.86	10.72
S22	0.99	16.74	20.19	19.25	31.69	6.32	27.16	10.32

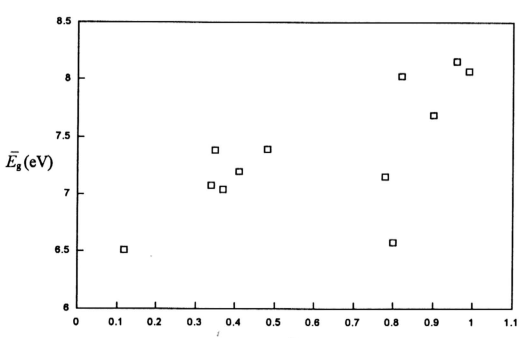

Figure 5.6: Average energy gap $\bar{E}_g$ versus x for ZnS_xSe_{1-x} films prepared by electron beam evaporation onto glass substrates at 60 °C.

and $\bar{E}_g$ is the important parameter for structural properties. The $\bar{E}_g$ is composed of contributions from the covalent or homopolar energy E_h and the ionic or heteropolar energy C in alloy systems [104,106]

$$\bar{E}_g^2 = E_h^2 + C^2 \quad \text{.....(5.5)}$$

The fractional covalent and ionic characters f_c and f_i are defined by

$$f_c = E_h^2/(E_h^2 + C^2) \quad \text{.....(5.6)}$$

$$f_i = C^2/(E_h^2 + C^2) \quad \text{.....(5.7)}$$

However, the more ionic crystals have NaCl structure, while the more covalent ones occur in the zinc-blende or diamond structures. The dividing point between octahedral and tetrahedral coordination is $f_i = 0.785 \pm 0.010$ [104,111]. The values of f_i for ZnS and ZnSe crystals with zinc-blende and wurtzite structures are reported to be 0.62 and 0.63, respectively [104, 111]. By averaging these two values [112], $f_i = 0.625$ was used to estimate the energy gaps E_h and C for ZnS_xSe_{1-x} films by using the relations 5.5-5.7, $f_c = 1 - f_i$. Figure 5.7 displays the variation of E_h and C with x. It was assumed that E_h scales with the cubic lattice constant a_0 according to a power law, E_h α a_0^s. For diamond structure, s value has been reported to be – 2.5 [111]. Figure 5.8 shows the variation of E_h with a_0 ,where s was found equal to -3.0, for ZnS_xSe_{1-x} films with zinc-blende structure. C represents the change in gap produced by the anti-symmetric potential in a binary compound, and is assumed to be independent of the

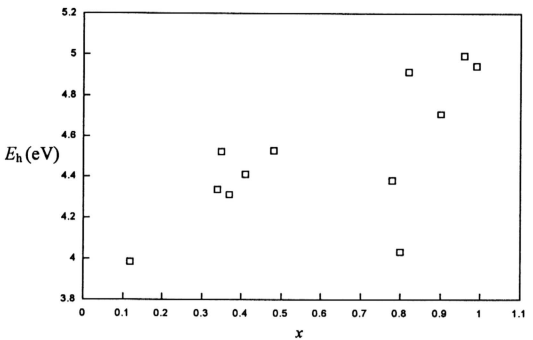

(a)

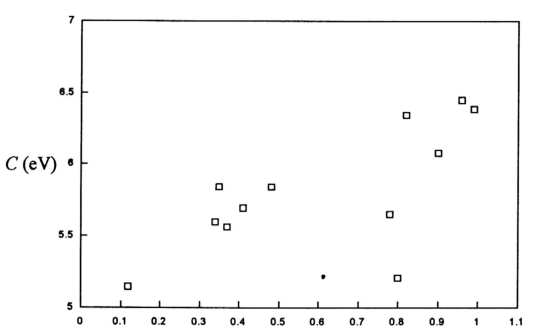

(b)

Figure 5.7: Covalent and ionic energy gaps, E_h and C, versus x for ZnS_xSe_{1-x} films Prepared by electron beam evaporation onto glass substrates at 60 °C.

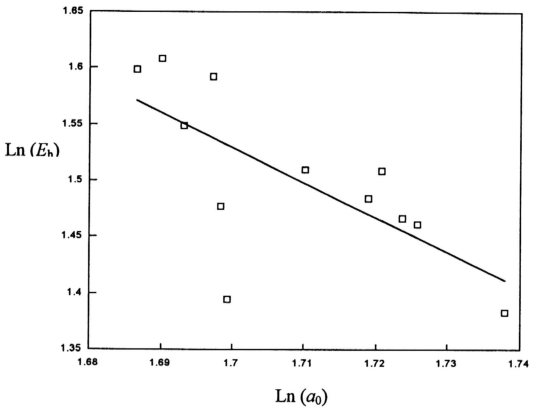

Figure 5.8: Ln (E_h) versus ln(a_0) for ZnS_xSe_{1-x} films prepared by electron beam evaporation onto glass substrates at 60 °C.

energy gap [113]. Moreover, $\bar{E}_g$ relates to E_F, which is the total valence electron Fermi energy measured from the zero energy of the bottom of the valence band. The typical value of $B_v = \bar{E}_g/4E_F$ is 0.1 [111]. This value along with $\bar{E}_g$ values were used to estimate E_F for ZnS_xSe_{1-x} films. The results are tabulated in Table 5.1. The average energy E_{av} of the valence electrons, which form the tetrahedral bonds, has been given [114] as

$$E_{av} - E_B = E_F[0.68 + 3B_v^2(1 + \ln(B_v/2)) - 4B_v^3] \quad \text{.....(5.8)}$$

where E_B is the energy level corresponding to the bottom of the valence band. E_{av} can be determined from equation 5.8 if one can determine the width of the valence band E_B. E_B relates to E_F and the heteropolar energy C through the relation [115]

$$E_B = \frac{E_F}{\sqrt{1+(C/E_F)^2}} \quad \text{.....(5.9)}$$

(where D in equation 5.135 in reference [115] was assumed to be 1.0 for ZnS_xSe_{1-x} films. This assumption was made by comparing equation 5.90 in reference [115] with equation 6 in reference [105]). The role of the heteropolar energy C is to narrow the valence band, just as it widens the average energy gap. Using the values of E_F and C for ZnS_xSe_{1-x} films, E_B was determined according to equation 5.9, subsequently, these values of E_B were used in equation 5.8 to determine E_{av}. The determined values of E_B and E_{av} for ZnS_xSe_{1-x} films are shown in Table 5.1.

In the region of transparency; the important inter-band transitions in the Brillouin zone (BZ) have been approximated by individual oscillators where each

valence electron contributes one such oscillator [105]. The energy dependence of the refractive index in this region is given [87, 105, 107] by

$$n^2(E) - 1 = E_o E_d/(E_o^2 - E^2) \quad \text{.....(5.10)}$$

where E_o is the energy of the effective dispersion oscillator, E is the photon energy and E_d is the so-called dispersion energy. The latter quantity measures the average strength of inter-band optical transitions. Figure 5.9 shows plots for $1/(n^2-1)$ versus E^2 for ZnS_xSe_{1-x} films. E_0 and E_d were estimated from the slopes and the intercepts of the plots and their values are included in Table 5.1. E_d has been found [87, 105] to obey the empirical relation

$$E_d = \beta N_c Z_a N_e \quad \text{.....(5.11)}$$

where N_c is the coordination number of the cations surrounding an anion, Z_a is the formal chemical anion valency and N_e is the effective number of valence electrons per anion. The constant β in equation 5.11 was found [105] to take two values for a wide variety of solids and liquids. For ionic materials, $\beta_i = 0.26 \pm 0.04$ eV and for covalent materials $\beta_c = 0.37 \pm 0.05$ eV. For the materials with zinc-blende structures, like ZnS_xSe_{1-x}, $N_c = 4$, $Z_a = 2$ and $N_e = 8$. By using these values in equation 5.11 along with E_d values in Table 5.1, β, in average, was found to be 0.45 eV for ZnS_xSe_{1-x} thin films.

The results of E_0 and E_d in Table 5.1 are in the range of the reported [105] values for zinc-blende crystals of ZnS ($E_0 = 6.36$ eV and $E_d = 26.1$ eV) and ZnSe ($E_0 =$

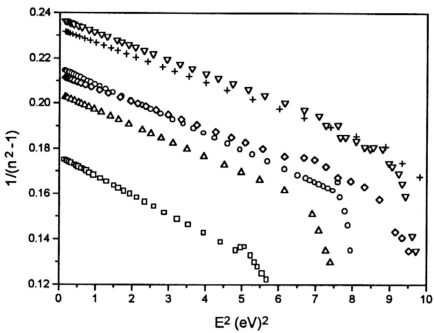

Figure 5.9: $1/(n^2\text{-}1)$ versus E^2 forZnS_xSe_{1-x} thin films prepared by electron beam evaporation onto glass substrates at 60 °C with x values 0.12 □, 0.35 ○, 0.41 △, 0.82 ▽, 0.90 ◇ and 0.99 +.

5.54 eV and E_d = 27.0 eV). According to equation 5.11, E_d depends on N_c, which for polycrystalline materials takes values different from those of crystalline materials because of the presence of incomplete or dangling bonds at the void boundaries. However, in tetrahedrally bonded materials, whether ionic or covalent, E_d remains largely unaffected by loss of long-range order that is the nearest neighbor environment remains largely intact [107]. It was also emphasized [105] that E_d is independent of the lattice constant (or density) of the solid.

Yet another energy-gap parameter E_a has been introduced by Hopfield [116] in a high-frequency sum rule relating optical properties to the charge distribution within a unit cell. However, E_a relates to E_p and E_d as $E_a = E_p^2/E_d$. The values of E_a for ZnS_xSe_{1-x} films are estimated and inserted in Table 5.1. Physically, E_a is the natural energy of the electronic charge clouds vibrating against the atomic cores.

5.4 Absorption coefficient and the fundamental energy gap

Figure 5.10 shows the absorption coefficient α (calculated from $\alpha = 4\pi k/\lambda$), for different ZnS_xSe_{1-x} films with different x values, as a function of the incident photon energy E. This Figure shows three distinct regions, the high-absorption region ($\alpha > 10^4$ cm^{-1}), the exponential part and the weak-absorption tail. As can be seen from the Figure, α shifts towards higher energies as the concentration of sulfur x increases in the films. This shift of α can be attributed to the corresponding shift of the fundamental optical energy gap as in the usual amalgamation-type mixed crystal [107]. The long tail appears in α values (Figure 5.10) below the energy gap could be due to the defects and grain size distribution in the film [116].

Basically there are two types of optical transmission that can occur at the fundamental absorption edge of the crystalline semiconductor, direct and indirect. Both

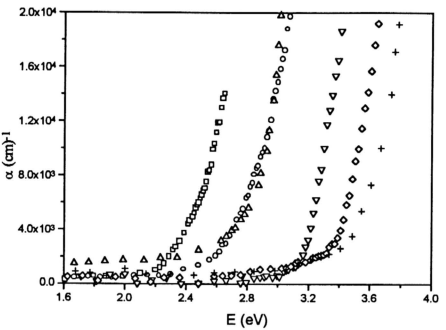

Figure 5.10: Absorption coefficient versus photon energy for ZnS_xSe_{1-x} thin films prepared by electron beam evaporation onto glass substrates at 60 ° C with x values: 0.12 □, 0.35 ○, 0.41 △, 0.82 ▽, 0.90 ◇ and 0.99 +.

involve the interaction of an electromagnetic wave with an electron in the valence band, which is raised across the fundamental gap to the conduction band. If the band edges involved are at the same point in the Brillouin zone so that the extremum of the exciton band is at **K** = 0, the transition is called direct, otherwise, it is an indirect one. However, indirect transitions also involve simultaneous interaction with lattice vibrations, which produces the annihilation or creation of phonons to balance the momentum change of the electron.

Indirect transitions can occur only when the perfection of the crystal is destroyed e. g. by lattice vibrations or impurities [3, 72]. For direct interband transitions (simple parabolic bands) in the absence of electron-hole interactions, the absorption coefficient α is given by [72]

$$\alpha nE \sim (E - E_g)^j \qquad (5.12)$$

where j = 1/2 or 3/2 depends on whether the transition is allowed or forbidden in the quantum-mechanical sense. E is the incident photon energy, E_g is the fundamental optical energy gap and n is the refractive index. For indirect transitions, where the phonon absorption and emission are involved in the transition process, α is expressed [70, 72] such that

$$\alpha nE = A' \frac{(E - E_{oi} + E_{ph})^j}{\exp\left(E_{ph}/K_\beta T\right) - 1} + \frac{(E - E_{oi} - E_{ph})^j}{1 - \exp\left(-E_{ph}/K_\beta T\right)} \qquad (5.13)$$

where j = 2 for allowed transitions and j = 3 for forbidden transitions, A' is a constant, E_{oi} and E_{ph} are, respectively the optical energy gap for the indirect transitions and the phonon energy, K_β is the Boltzmann constant and T is the absolute temperature. The

first term in the right hand side of equation 5.13 represents the phonon absorption while the second term represents the phonon emission in the transition process.

Since both ZnS and ZnSe are direct band gap semiconductors, the fundamental absorption edge in the high absorption region was fitted to the direct transition expression (equation 5.12) and the plots of $(\alpha nE)^2$ and $(\alpha nE)^{2/3}$ versus E for various compositions are shown in Figures 5.11 (a) and (b), respectively. The linear behaviour of the plots in the high absorption region confirms the direct nature of the fundamental transition in ZnS_xSe_{1-x} system. The fundamental optical energy gap E_g was estimated from the intercepts of the plots in Figure 5.11 (a) with the energy axis. These values of E_g are plotted in Figure 5.12 as a function of x for ZnS_xSe_{1-x} films. It can be seen that E_g changed from 2.583 eV (for $x = 0.12$) to 3.725 eV (for $x = 1.0$). However, a linear variation of energy gap $E_g(x)$ with composition has been found [49] for ZnS_xSe_{1-x} system. In contrast, $E_g(x)$ for AB_xC_{1-x} semiconductor system was found to deviate from the linear dependence on x, instead $E_g(x)$ varies with x in a quadratic relation such as

$$E_g(x) = E_{g(AC)} + (E_{g(AB)} - E_{g(AC)} - p)x + px^2 \quad \text{.....(5.14)}$$

where $E_{g(AC)}$ and $E_{g(AB)}$ represent the energy gaps of AB and AC materials, respectively, and p is the optical bowing parameter. $E_g(x)$ for solid solutions of zinc chalcogenides ZnS_xSe_{1-x}, ZnS_xTe_{1-x} and $ZnSe_xTe_{1-x}$ were found to follow equation 5.14 with bowing parameter ($p \sim 0.06$ eV for ZnS_xSe_{1-x}, see references in [41], $p \sim 2.4$ eV for ZnS_xTe_{1-x} [49] and $p \sim 1.3$ eV for $ZnSe_xTe_{1-x}$ [49]). For the purpose of comparison, the linear behavior of $E_g(x)$ reported in [49] and the bowing results reported in [51] are plotted with the results obtained in this work in Figure 5.12. The composition dependence of $E_g(x)$ and the observed optical bowing have been studied theoretically in attempts to

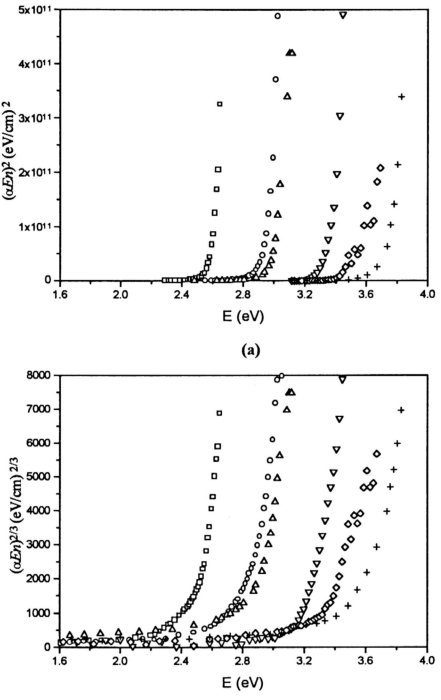

Figure 5.11: $(\alpha nE)^2$ **(a)** and $(\alpha nE)^{2/3}$ **(b)** versus E forZnS_xSe_{1-x} thin films prepared by electron beam evaporation onto glass substrates at 60 ° C with x values: 0.12 □, 0.35 ○, 0.41 △, 0.82 ▽, 0.90 ◇ and 0.99 +.

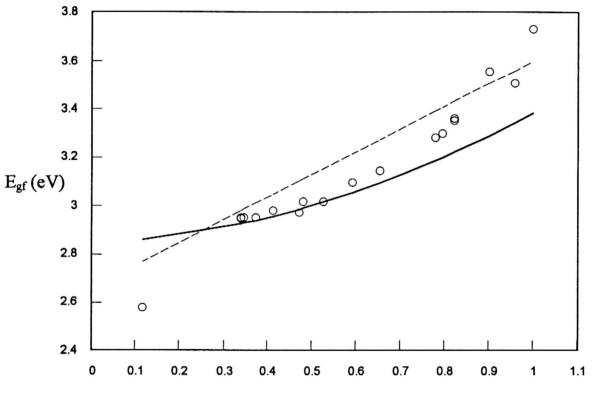

Figure 5.12: Fundamental optical energy gap E_{gf} versus x for ZnS_xSe_{1-x} thin films: this work (open circles), dashed line from [40] and solid line from [67].

find a simple relation between these quantities. These studies have been intensively reviewed in reference [41] and will not be discussed here. It is sufficient to mention here that the most prevailing approach to the problem is the virtual-crystal approximation (VCA), in which the individuality of B and C elements in the alloy system is replaced by an average "virtual" element $< BC >$, and the disorder effect, are not taken into account. Despite the existence of bowing parameter which is small in ZnS_xSe_{1-x} system compare to other systems, the energy gap of the films studied in this work are in the range of that values reported previously (see Figure 5.12).

However, the existence of uniaxial stress inside the material may cause a shift and a splitting of the energy band edges, *viz.*, the top of the valence band, and as a result the energy gap of the free-stress material will take different values if this material is subjected to a sort of stress. The value of the energy gap E_g as a function of uniaxial strain parallel to the $< 111 >$ direction in zinc-blende-type semiconductor, for the first order in the stress formula, is given by [117, 118]

$$E_g^{<111>} = E_g + \delta E_H - (1/2)\delta E_{<111>} \quad \text{.....(5.15)}$$

where

$$\delta E_H = a`(S_{11} + 2S_{12})SS \quad \text{.....(5.16)}$$

is the shift of the gap E_g due to the hydrostatic component of the strain and

$$\delta E_{<111>} = 3^{-1/2} d` S_{44} SS \quad \text{.....(5.17)}$$

is the linear splitting of the $P_{3/2}$ multiplet, S_{ij} are the elastic compliances, SS is the magnitude of the <111> stress, a' and d' are the deformation potentials. By using the deformation potentials of ZnS [6, 118] and ZnSe [119] materials given in Table 5.2, the deformation potentials of ZnS_xSe_{1-x} materials were determined (see Table 5.3) by assuming a linear interpolation between those of ZnS and Znse [120]. Using these values of a' and d' along with S_{ij} and SS values determined previously in Table 4.8 (chapter 4), δE_H and $\delta E_{<111>}$ were estimated (using equations 5.16 and 5.17) for ZnS_xSe_{1-x} thin films under investigation and tabulated in Table 5.3. Note that in Table 4.8 (chapter 4) the positive sign was given to the tensile stress while negative sign to the compressive stress, according to the definition of the strain followed in this work. Since SS with positive sign, in Equations 5.16 and 5.17, refers to compressive stress so the signs of SS values in Table 4.8 have to be reversed. The shift in the energy gap δE_g (= δE_H - (1/2)$\delta E_{<111>}$) due to the stress ranges from –0.54 meV to 0.62 meV (see Table 5.3). The negative sign means that the stress causes a shift in the top of the valence band towards higher energies while positive sign means a recession of the top of the valence band towards lower energies occurred.

Besides the effect of the stress on the energy gap, quantum size effect may also have an important contribution to the value of E_g of a microcrystalline semiconductor. This effect, which is known as quantum-confined effect, manifests itself when the microcrystalline size approaches the exciton Bohr radius. For II-VI semiconductors, the Bohr radii are typically in the range of 20-80 Å [121]. It has been suggested that as the crystallite approaches this size, the electron and hole interactions with the crystallite surface will dominate the dynamics and the energy level scheme will depend upon the size and shape of the crystallite as well as the nature of the material [122].

Table 5.2: Deformation potentials of ZnS [6, 118] and ZnSe [119] materials.

	Deformation potentials (eV)		
	a`	b`	d`
ZnS	-5.0	-0.53	-3.7
ZnSe	-5.4	-1.2	-3.8

Table 5.3: Deformation potentials, shift in E_g caused by the stress (δE_H and $\delta E_{<111>}$), reduced effective mass, shift in E_g caused by grain size effect (ΔE_g) and the estimated crystal energy gap for ZnS_xSe_{1-x} materials.

Sample	x	Deformation potentials (eV)			δE_H (meV)	$\delta E_{<111>}$ (meV)	δE_g (meV)	μ^* $\times m_e$	ΔE_g (meV)	E_{gs} (eV)
		a`	b`	d`						
S1	0.12	-5.35	-1.12	-3.79	47.1	93.0	0.62	0.141	2.43	2.58
S2	0.34	-5.26	-0.97	-3.77	25.5	50.8	0.06	0.166	2.57	2.95
S3	0.35	-5.26	-0.97	-3.77	12.1	24.2	0.02	0.167	6.13	2.94
S4	0.37	-5.25	-0.95	-3.76	43.3	86.5	0.04	0.170	3.84	2.95
S5	0.41	-5.24	-0.93	-3.76	17.4	34.7	-0.02	0.174	7.37	2.97
S6	0.48	-5.21	-0.88	-3.75	-11.4	-22.9	0.05	0.182	33.02	2.99
S7	0.78	-5.09	-0.68	-3.72	1.2	2.4	-0.02	0.216	11.12	3.27
S8	0.8	-5.08	-0.66	-3.72	10.8	22.0	-0.23	0.218	0.72	3.30
S9	0.82	-5.07	-0.65	-3.72	5.0	10.2	-0.11	0.221	2.40	3.35
S10	0.90	-5.04	-0.60	-3.71	-0.1	-0.3	0.01	0.230	8.33	3.55
S11	0.90	-5.04	-0.60	-3.71	1.4	3.0	-0.04	0.230	2.11	3.55
S12	0.90	-5.04	-0.60	-3.71	3.8	7.7	-0.10	0.230	5.14	3.55
S13	0.90	-5.04	-0.60	-3.71	11.5	23.6	-0.30	0.230	7.07	3.55
S14	0.90	-5.04	-0.60	-3.71	3.2	6.5	-0.08	0.230	14.39	3.55
S15	0.90	-5.04	-0.60	-3.71	2.4	4.9	-0.06	0.230	6.07	3.55
S16	0.90	-5.04	-0.60	-3.71	20.6	42.2	-0.54	0.230	0.23	3.55
S17	0.90	-5.04	-0.60	-3.71	-0.9	-1.9	0.02	0.230	4.09	3.55
S18	0.90	-5.04	-0.60	-3.71	-7.8	-15.9	0.02	0.230	8.16	3.55
S19	0.90	-5.04	-0.60	-3.71	-5.5	-11.2	0.14	0.230	3.16	3.55
S20	0.90	-5.04	-0.60	-3.71	7.8	15.9	-0.20	0.230	8.05	3.55
S21	0.96	-50.2	-0.56	-3.70	2.8	5.8	-0.08	0.237	12.67	3.49
S22	0.99	-5.00	-0.54	-3.70	-7.3	-15.1	0.23	0.242	4.89	3.72

The shift in E_g, which can be caused by the crystallite size, was given [122] in the effective mass approximation such as

$$\Delta E_g = \frac{2\hbar^2\pi^2}{D^2}\left[\frac{1}{m_e^*}+\frac{1}{m_h^*}\right] = \frac{2\hbar^2\pi^2}{D^2\mu^*} \quad \text{.....(5.18)}$$

Where D is the crystallite diameter, m_e^* and m_h^* are the effective masses of the electron and hole respectively and $\mu^* = m_e^* m_h^*/(m_e^* + m_h^*)$ is the effective reduced mass. Figure 5.13 (a) shows the energy gap variation with crystallite diameter for $ZnS_{0.9}Se_{0.1}$ films. The solid line in Figure 5.13 (a) was obtained by fitting the experimental data to the theoretical expression given by Brus [122] as

$$E_{gf} = E_{gc} + \Delta E_g \quad \text{.....(5.19)}$$

where E_{gf} and E_{gc} are the energy gaps of the film and the bulk materials, respectively, ΔE_g was given in equation 5.18. By taking into consideration the stress effects on the energy gap (equation 5.15), expression 5.19 can be rewritten as

$$E_{gf} = E_{gc} + \Delta E_g + \delta E_g \quad \text{.....(5.20)}$$

By plotting E_g versus $1/D^2$ (as shown Figure 5.13 (b)), the energy gap E_{gc} and the effective reduced mass μ^* for $ZnS_{0.9}Se_{0.1}$ crystal were estimated according to equation 5.19 and found to be E_{gc} = 3.547 eV and μ^*=0.230 m_e, where m_e is the electron rest mass. It has been reported [123] that μ^* for ZnS and ZnSe semiconductors are 0.242 m_e and 0.128 m_e, respectively. By assuming that μ^* varies linearly with x for ZnS_xSe_{1-x} semiconductors, μ^* will equal to 0.231 m_e for $ZnS_{0.9}Se_{0.1}$, which is in a good agreement

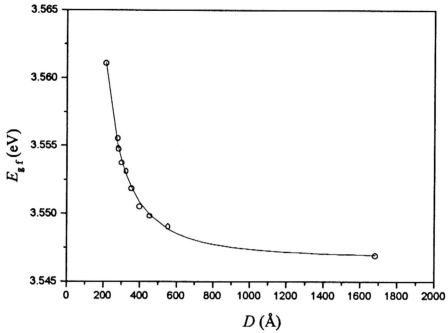

(a)

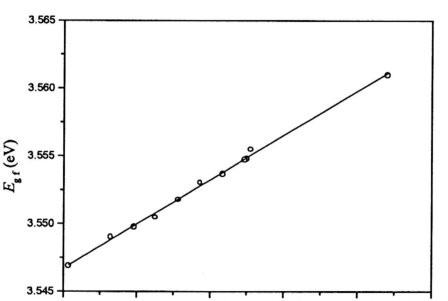

(b)

Figure 5.13: Energy gap (E_{gf}) versus micro-crystallite diameter D **(a)** and $1/D^2$ **(b)** for $ZnS_{0.9}Se_{0.1}$ thin films prepared by electron beam evaporation onto glass substrates at 60 ^{0}C.

with the values obtained from Figure 5.13 (b). By adopting the assumption of the linear variation of μ^* with x, μ^* was estimated for ZnS_xSe_{1-x} materials and the shift in E_g caused by the crystallite size effect (i. e. ΔE_g), according to equation 5.18, together with the energy gap for the corresponding crystals E_{gc}, according to equation 5.20, were estimated. μ^*, ΔE_g and E_{gc} are listed in Table 5.3.

From the variation of the absorption coefficient α with the incident photon energy E, as shown in Figure 5.10, the exponential edge, which is known as Urbach edge, is observed for ZnS_xSe_{1-x} samples studied in this work. In this region, a gradual increase in α extending over several eV is usually observed. α in this region is given [124, 125] by

$$\alpha = \alpha_0 \exp\left\{\gamma_0 \left[E - E_0(T)\right] / K_\beta T^*\right\} \quad \text{.....(5.21)}$$

where α_0 and γ_0 are constants, K_β is Boltzmann constant, $E_0(T)$ is the temperature-dependent gap and T^* is the effective temperature [125], which is almost constant below a critical value T_0 and is proportional to T at high temperature (above T_0). By plotting $\ln(\alpha)$ versus E, as shown in Figure 5.14, the slope $(d(\ln\alpha)/dE)$ gives $\gamma_0/K_\beta T^*$, which indicates that the sharp absorption edge becomes broader as the temperature rises above T_0 [124]. This region is strongly related to the impurity concentrations of the sample [70]. It has been pointed out that γ_0 varies linearly with temperature so that the ratio $\gamma_0/K_\beta T^*$ is constant for amorphous and polycrystalline materials and it is temperature dependant for pure single crystals [125]. The ratio $\gamma_0/K_\beta T^*$ was estimated for ZnS_xSe_{1-x} films and tabulated in Table 5.4.

The tail in the absorption coefficient (see Figure 5.10) close to the band edge is associated with phonon-assisted transitions. Its strength and shape depend on the

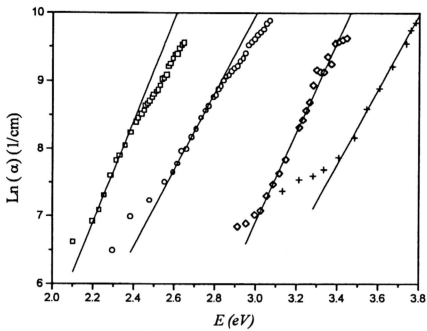

Figure 5.14: Ln(α) versus E, in the exponential part of the absorption coefficient, for ZnS_xSe_{1-x} thin films prepared by electron beam evaporation onto glass substrates at 60 ^{0} C with x values: 0.12 □, 0.35 ○, 0.90◇ and 0.99 +.

Table 5.4: $\gamma_0/K_\beta T^*$ parameters and optical phonon energies for ZnS_xSe_{1-x} thin films prepared by electron beam evaporation onto glass substrates at 60 ° C.

Sample	x	$\gamma_0/K_\beta T^*$ (1/eV)	E_{ph1} (meV)	E_{ph2} (meV)	E_{ph3} (meV)
S1	0.12	7.50	95	210	407
S2	0.34	5.76	183	355	843
S3	0.35	5.71	229	424	--------
S4	0.37	7.62	64	264	--------
S5	0.41	6.79	100	210	650
S6	0.48	4.51	177	810	--------
S7	0.78	4.96	136	252	454
S8	0.8	5.62	67	306	786
S9	0.82	4.80	47	269	438
S10	0.90	6.95	79	180	518
S11	0.90	7.54	143	601	--------
S12	0.90	3.48	341	843	--------
S13	0.90	5.85	178	258	--------
S14	0.90	5.36	123	235	443
S15	0.90	4.77	94	166	494
S16	0.90	7.64	157	237	--------
S17	0.90	8.53	48	146	673
S18	0.90	7.52	70	57	258
S19	0.90	6.67	41	188	391
S20	0.90	5.41	107	194	548
S21	0.96	8.43	58	206	358
S22	0.99	5.53	58	136	301

preparation, purity and thermal history and also on the thickness of the sample [125]. Figure 5.15 shows the relation between $(\alpha En)^{1/2}$ and E for different ZnS_xSe_{1-x} samples. By extrapolating the linear portion in Figure 5.15 to the energy axis where $\alpha = 0$, one can estimate E_{oi}, which is the optical energy gap for the indirect transition. In the region where $E < E_{oi}$, the dependence of α on E obeys equation 5.13 (assuming allowed indirect transitions, i. e. j = 2, with assistance of phonon absorption) as

$$\alpha En = \frac{A'\left(E - E_{oi} + E_{ph}\right)^2}{\exp\left(E_{ph}/K_B T\right) - 1} \qquad \text{.....(5.22)}$$

The value of the phonon energy E_{ph} can be obtained from the above equation (equation 5.22) such that $E_{ph} = E_{oi} - E$ at $\alpha = 0$ (see Figure 5.16 for $ZnS_{0.12}Se_{0.88}$). The extrapolations of the linear portions of the tail to $\alpha = 0$ in Figure 5.16 give phonon energies of 95, 210 and 407 meV corresponding to optical phonon wave numbers 766, 1694 and 3283 cm^{-1}, respectively. The optical phonon energies E_{ph1}, E_{ph2} and E_{ph3} are estimated for ZnS_xSe_{1-x} films and tabulated in Table 5.4. Transitions with phonon assistance have been observed in ZnSe samples [125] with energies of 25, 75 and 120 meV.

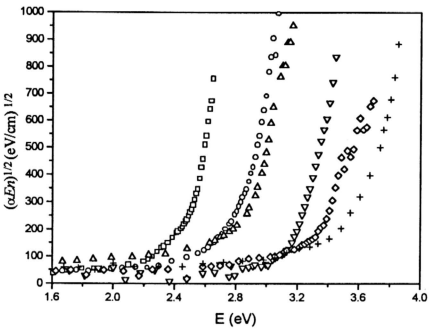

Figure 5.15: $(\alpha En)^{1/2}$ versus E for ZnS_xSe_{1-x} thin films prepared by electron beam evaporation onto glass substrates at 60 ° C with x values: 0.12 □, 0.35 ○, 0.41△, 0.82▽, 0.90 ◇ and 0.99 +.

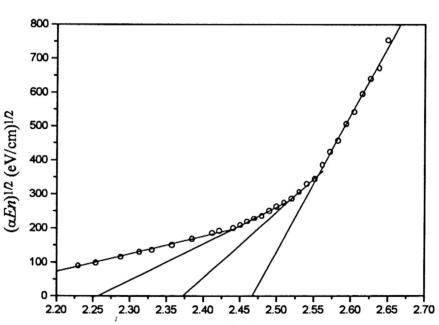

Figure 5.16: $(\alpha nE)^{1/2}$ versus E for $ZnS_{012}Se_{0.88}$ thin film prepared by electron beam evaporation onto glass substrate at 60 ° C.